

# A Pilot Plant Study of Coal Dryer: Simulation and Experiment

**Abdul Halim** \*<sup>1</sup>

**Afninda Aryuni Widyanti** <sup>1</sup>

**Celvin Dicky Wahyudi** <sup>1</sup>

**Fahimah Martak** <sup>2</sup>

**Eka Luthfi Septiani** <sup>1,3</sup>

<sup>1</sup> Department of Chemical Engineering, Universitas Internasional Semen Indonesia, Kompleks PT. Semen Indonesia (Persero) Tbk, Jl. Veteran, Kb. Dalem, Sidomoro, Kebomas, Gresik, Jawa Timur, Indonesia 61122

<sup>2</sup> Department of Chemistry, Faculty of Science, Institut Teknologi Sepuluh Nopember, Jl. Raya ITS, Surabaya, Jawa Timur, Indonesia

<sup>3</sup> Department of Chemical Engineering, Faculty of Engineering, Hiroshima University, 1-4-1 Kagamiyama, Higashi Hiroshima, Japan, 739-8527

\*e-mail: [abdul.halim@uisi.ac.id](mailto:abdul.halim@uisi.ac.id)/[abdul-halim.xm@alumni.tsukuba.ac.jp](mailto:abdul-halim.xm@alumni.tsukuba.ac.jp)

*Submitted* 29 August 2021

*Revised* 06 Januari 2021

*Accepted* 19 March 2022

---

**Abstract.** High moisture content in low-range coal causes low calorific value. To increase the quality, drying by a coal dryer to minimize moisture content is proposed. Here, a case study of a cyclone-like conical tube coal dryer pilot plant was reported. Drying heating uses combustion heat generated from volatile matter combustion. This approach will solve the two problems simultaneously: decreasing moisture content and volatile matter. The computational fluid dynamic (CFD) approach is used to study fluid dynamics inside the coal dryer using ANSYS Fluent 2020R2 software. The CFD simulation results represent the phenomenon of coal drying inside the coal dryer validated by the pilot plant experimental result. The simulation was carried out in steady and unsteady conditions to understand the drying phenomena. The simulation firmly fits the experimental result, especially in an unsteady state system, indicating that the simulation result is promising for further coal dryer design. The optimal condition produces a high moisture content reduction of 86.37%, uniform fluid distribution, and significant volatile matter combustion.

**Keywords:** Coal Upgrading, Coal dryer, CFD Simulation, Case Study, Unsteady state

## INTRODUCTION

Coal generates 40% of electricity in the world (Yadav and Mondal 2019). The potential for coal in Indonesia reached 26.2 billion tons, and coal production reached 461 million tons in 2017 (ESDM 2018). The quality of coal in Indonesia is dominated by middle

to lower-quality coal. Coal with poor quality generally has a low heating value due to the high water content, so a processing technology is needed to improve coal quality. This is due to the high demand for coal in the future to meet domestic energy needs.

Low-range coal has a high moisture content of around 15-30% and a low calorific

value, which is less than 5000 kcal/kg (Baaqy et al., 2013). Low-quality coal causes higher coal consumption and more expensive production costs. The coal quality also affects the quality of industrial products. For instance, the cement clinker product is affected by the temperature generated by coal combustion inside the kiln (Canbek and Erdoğan, 2020; Yang et al., 2021). Therefore,

reducing the coal moisture content increases the coal quality to increase efficiency, heating rate, heating value, and industrial product quality. One technique to reduce moisture content is thermal coal drying (Osman et al., 2011). Thermal coal drying is the most straightforward drying technology and increases the heating value (Li et al., 2019).

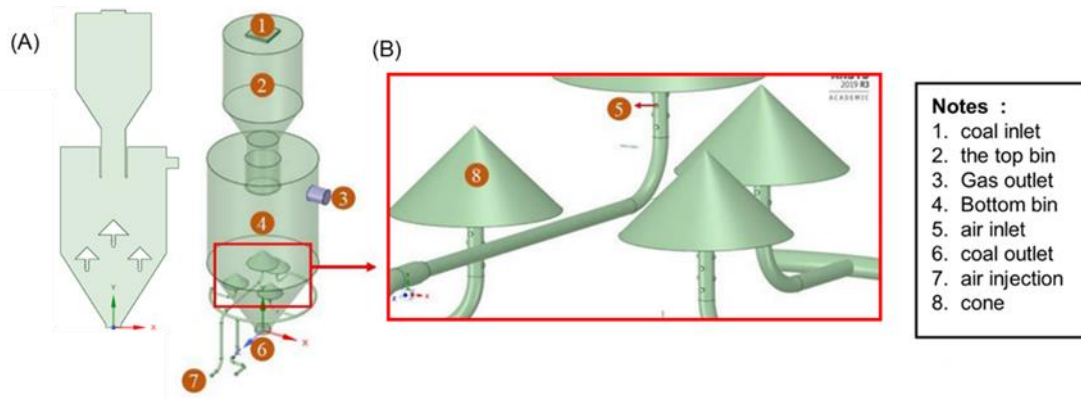


**Fig. 1:** 3D design of coal dryer (a) and magnification view of coal dryer (b)

**Table 1.** Comparison of several dryer type

| Dryer type               | Capital and operating cost | Thermal efficiency | Advantages   | Ref.   |
|--------------------------|----------------------------|--------------------|--|--|
| Fluidized bed            | Low                        | High               | Good mixing makes intensive and high efficiency      | Rao et al. 2015; Li et al. 2018; Phiciato and Yaskuri 2019 |
| Rotary dryer             | Medium                     | Medium             | Low fire hazard. Relatively established              | Rao et al. 2015; Li et al. 2018; Phiciato and Yaskuri 2019 |
| Hot oil-immersed drying, | High                       | High               | Good for low range coal. Very high energy efficiency | Rao et al. 2015; Ohm et al. 2012                           |
| Microwave drying         | High                       | High               | Faster drying rate                                   | Rao et al. 2015; Si et al. 2019                            |

**Table 2.** Variables used in this study

| Variable | Coal flow rate<br>(kg/s) | Air velocity<br>(m/s) | (+) %Excess or<br>(-) %lean | Equivalence<br>ratio |
|----------|--------------------------|-----------------------|-----------------------------|----------------------|
| A        | 5.95                     | 43.75                 | 143.23                      | 0.63                 |
| B        | 6.51                     | 43.75                 | 101.20                      | 0.68                 |
| C        | 7.06                     | 43.75                 | 70.10                       | 0.74                 |
| D        | 5.95                     | 29.96                 | 22.27                       | 0.91                 |
| E        | 6.51                     | 29.96                 | 0.00                        | 1.00                 |
| F        | 7.06                     | 29.96                 | -15.81                      | 1.08                 |
| G        | 5.95                     | 24.87                 | -34.80                      | 1.10                 |
| H        | 6.51                     | 24.87                 | 47.74                       | 1.20                 |
| I        | 7.06                     | 24.87                 | -56.34                      | 1.31                 |

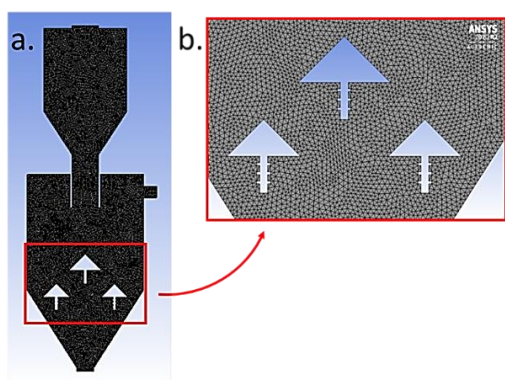


**Fig. 2:** (a) Meshing result of grid coal dryer.  
(b) Enlargement of distribution result of grid coal dryer.

The thermal evaporative drying is conducted in a fluidized bed, rotary drying, hot oil-immersed drying, and microwave drying (Rao et al. 2015). Table 1 summarizes the specification of each drying type. Fluidized beds efficiently reduced the moisture content to 11-12%, depending on the coal type and operating condition. Rotary drying is a relatively established technology applied in a wide area. Both fluidized bed and rotary drying need an energy source, usually from flue gas (Phiciato and Yaskuri 2019) or steam (Li et al. 2018) for indirect contact or direct contact drying, respectively. Hot oil-immersed drying uses hot oil to evaporate moisture content (Ohm et al. 2012). This

technology is frequently referred to as fry drying. Microwave drying uses microwave energy to evaporate moisture content (Si et al. 2019).

Among thermal evaporative drying, fluidized bed and rotary drying are mainly used successfully in the industry (Rao et al. 2015). However, rotary drying and fluidized bed are less energy-efficient (Rao et al. 2015) and insufficiently remove volatile matter of coal. Coal drying and power plant integration were proposed to increase the energy and volatile matter removal efficiency (Liu et al. 2020). Therefore, direct contact drying by utilizing volatile matter is expected to produce higher drying efficiency. The volatile matter of coal will be burned to generate heat and contact with the drying coal directly.

Even though direct contact drying produces high thermal efficiency, the control process is difficult. The drying efficiency is affected by dryer media, coal condition, and dryer design. The evaporation mechanism will affect the drying time to dictate the effluent coal moisture content (Li et al. 2017). Thus, understanding the chemical and physical phenomena inside of the dryer is necessary.

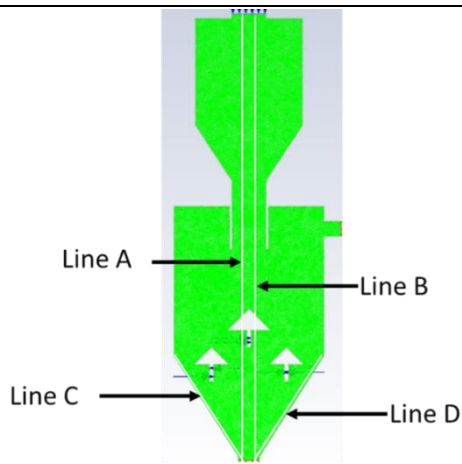


**Fig. 3:** Location of the 1-dimensional line of observation of Moisture Content Fraction through Lines A, B, C, D

Direct experimental of coal dryers is costly and limited to observing the phenomena of combustion and drying. One of the efforts to answer this problem is by conducting numerical simulation using the Computational Fluid Dynamic (CFD) method (Halim et al. 2013, 2014; Siripaiboon et al. 2020). Several previous research has reported the numerical simulations in several drying unit operations (Zhang and You 2013; Xu et al. 2018; Si et al. 2019; Simanjuntak et al. 2019; Auamwong and Srinophakun 2020). However, a numerical study of coal dryers validated by the experimental result of a pilot plant is rarely reported.

Herein, a direct contact coal dryer that utilizes heat generated by volatile matter combustion to decrease moisture content was proposed. The CFD simulation by solving the momentum, heat, and mass balance equation was conducted using ANSYS Fluent 2020 R2. By this simulation, the fluid dynamic inside of the coal dryer can be easily observed. Simulations are carried out under conditions of excess, theoretical, and air-lean conditions. The H<sub>2</sub>O levels, carbon, and CO<sub>2</sub> concentration will be observed in this study.

Our simulation fits very closely to the pilot plant result indicating that our simulation method can be applied to further coal dryer design.

## EXPERIMENTAL

### Model development, the initial and boundary conditions

Figure 1 shows the coal dryer design and geometry based on our pilot plant (the detailed geometry is shown in Figure S1). The thermocouple was placed in the middle of the bottom bin. This coal dryer consists of 2 parts. The upper part is temporal coal storage to supply coal steadily. The drying process occurs in the coal dryer's lower position. Coal dryer geometry was drawn using SpaceClaim software, followed by meshing using Ansys Meshing software. The meshing process was carried out in a triangle/triangle, as shown in Figure 2. The skewness value reviews the meshing quality. The quality of meshing is excellent if the skewness value is less than 0.25. The meshing produces 11,093 points with the number of elements 21,326 with an average skewness value of  $5.16 \times 10^{-2}$ , revealing an excellent meshing result (ANSYS Inc. 2020).

After that, modeling was carried out in the Ansys Fluent software. The modeling solution uses a pressure-based solver type by activating the gravitational force. Pressure-based solver type suits compressible flow (Jovanovic et al. 2011). The viscous modeling is by selecting k-epsilon realizable. The realizable k-epsilon type was chosen because it provides the best computational performance compared to other complex turbulent flow validation (ANSYS Inc. 2020). Then, modeling reactions using species transport through the convection-diffusion equation.

Furthermore, the material selection is carried out by defining the fluid as air. A mixture of coal-volatile matter-air was used as input materials. Coal was set as a droplet particle (coal diameter, 3 cm). The sub-bituminous coal characteristic data is entered according to (Grimes et al. 1990). We used the Discrete Phase Model because the system consists of two phases: the continuum fluid phase and the discrete dispersed phase. The dispersed phase is solved by tracing many particles, bubbles, or droplets through the calculated flow plane. The dispersed phase can exchange momentum, mass, and energy with the fluid phase. This model assumes that the dispersed phase occupies a low volume fraction of less than 10%, so the modeling is suitable for modeling coal burning/drying.

The ratio of coal flow rate to the airflow rate as in Table 2 is set to be excess (0.63-0.91), stoichiometric point (1.00), and thin air (1.08-1.31). The characteristics of the simulated coal are in Table 3. The proximate analysis and ultimate analysis were from the previous report (Grimes et al. 1990).

**Table 3.** Coal parameters.

| Proximate analysis | Ultimate analysis |   |      |
|--------------------|-------------------|---|------|
| Volatile matter    | 0.3               | C | 0.85 |
| Fixed carbon       | 0.4               | H | 0.10 |
| Ash                | 0.0               | O | 0.04 |
| Moisture content   | 0.3               | N | 0.01 |
| Coal diameter      | 3 cm              |   |      |

In this study, the steady-state and unsteady-state were simulated using the Semi-Implicit Method for Pressure-Linked Equations Consistent (SIMPLEC) and the Pressure-Implicit with Splitting of Operators (PISO) algorithm, respectively. SIMPLEC algorithm leads the convergent fast even though simulating complicated flow

involving turbulence or additional physical models. PISO suits unsteady simulation and can maintain stable calculations even high the Under Relaxation Factor. Furthermore, Spatial Discretization uses a second order to minimize the numerical discretization error (ANSYS Inc. 2020).

The numerical calculation iteration was carried out until the iteration error value was 0.0001. We conducted two validations: coal combustion validation and pilot plant validation. Coal combustion validation used experimental data from Hankalin et al. (2011), as cited in Arena (2013), which the relationship between equivalent ratio to temperature under adiabatic conditions. Adiabatic conditions are the maximum temperature produced by the product of a combustion reaction if there is no heat leakage to the environment. Pilot plant validation was conducted on the Semen Indonesia research facilities. The coal dryer temperature was measured by a thermocouple sensor mounted on the bottom side of the air inlet cone. The data obtained by the thermocouple is then sent to the Computer Control System for recording temperature data every 20 seconds.

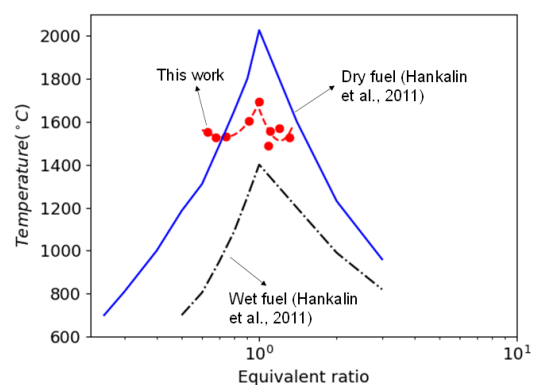


**Fig. 4:** Graph of the relationship between the Equivalence Ratio and the temperature of the adiabatic temperature conditions

After simulation, the temperature, moisture content, and CO<sub>2</sub> concentration distribution profile are analyzed in 2-dimensional observations and 1-dimensional observations through a line, as shown in Figure 3.

### Equations

In this simulation, the Multiphase Lagrangian Discrete Phase Model (DPM) was used. The CFD simulation method solves the conservation of mass (Eq. (1)), momentum (Eq. (2)), energy (Eq. (3)), and species transport equations (Eq. (4)).

$$\frac{\partial \rho}{\partial t} + \nabla \cdot (\rho \vec{v}) = S_m \quad (1)$$

$$\frac{\partial(\rho \vec{v})}{\partial t} + \nabla \cdot (\rho \vec{v} \vec{v}) = -\nabla p + \nabla \cdot (\vec{\tau}) + \rho \vec{g} + \vec{F} \quad (2)$$

$$\frac{\partial}{\partial t}(\rho E) + \nabla \cdot (\vec{v}(\rho E + p)) = \nabla \cdot (k_{eff} \nabla T - \sum_j h_j \vec{J}_j + (\vec{\tau}_{eff} \cdot \vec{v})) + S_h \quad (3)$$

$$\frac{\partial}{\partial t}(\rho Y_i) + \nabla \cdot (\rho \vec{v} Y_i) = \nabla \cdot \vec{J}_i + R_i + S_i \quad (4)$$

For Eq. (3), the first term is a conduction heat transfer, the second term is a species heat transfer by diffusion, and the third term is a stress tensor or heat loss through viscous dissipation (Marshall and Bakker 2003). The species transport equation predicts the mass fraction of each species with the diffusion-convection principal approach of each material (Marshall and Bakker 2003). We use k-ε model to simulate the flow turbulences (Eqs. (5-6)). The k model detects the flow through the particle's kinetic energy and the ε model uses the principle of reducing the particle energy level. The k turbulence kinetic energy and ε is the energy's rate of dissipation.

$$\frac{\partial}{\partial t} (pk) + \frac{\partial}{\partial x_i} (pk u_i) = \frac{\partial}{\partial x_j} \left[ \left( \mu \frac{\mu_t}{\sigma_k} \right) \frac{\partial k}{\partial x_j} \right] + G_k + G_b + \rho \varepsilon - Y_M + S_k \quad (5)$$

$$\frac{\partial}{\partial t} (p\varepsilon) + \frac{\partial}{\partial x_i} (p\varepsilon u_i) = \frac{\partial}{\partial x_j} \left[ \left( \mu \frac{\mu_t}{\sigma_\varepsilon} \right) \frac{\partial \varepsilon}{\partial x_j} \right] + C_{1\varepsilon} \frac{\varepsilon}{k} (G_k + C_{3\varepsilon} G_b) - C_{2\varepsilon} \rho \frac{\varepsilon^2}{k} + S_\varepsilon \quad (6)$$

## RESULTS AND DISCUSSION

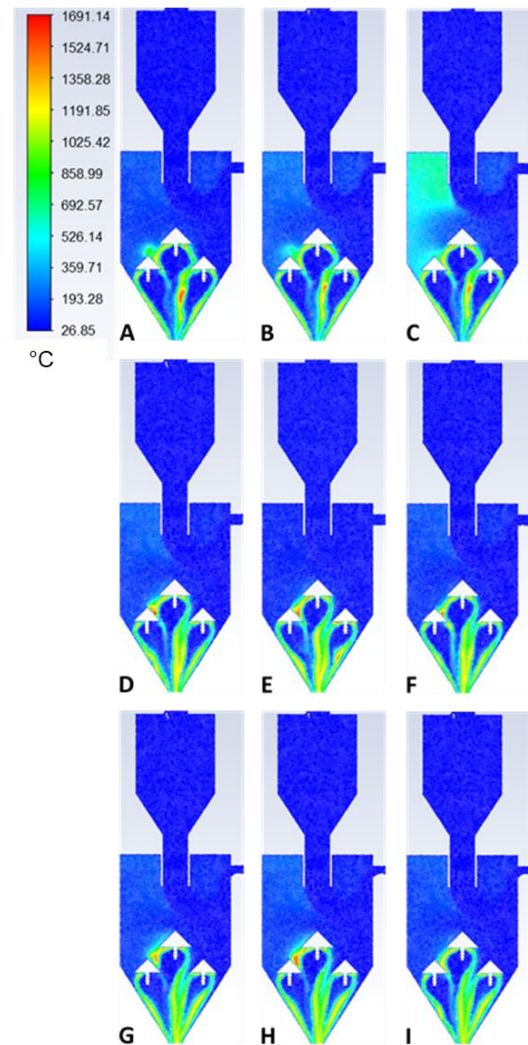


**Fig. 5:** Temperature distribution of variable A (ER 0.63), B (ER 0.68), C (ER 0.74), D (ER 0.91), E (ER 1), F (ER 1.08), G (ER 1.1), H (ER 1.2), I (ER 1.31) in the steady-state condition

### Modeling validation based on the effect of equivalence ratio on the temperature in coal dryer

Figure 4 shows the relationship between the equivalence ratio to the temperature of our simulation results and Hankalin's experimental results (Hankalin et al. 2011; Arena 2013). The equivalence ratio is defined as

$$\phi = \frac{\text{actual coal mass/actual air mass}}{\text{stoichiometric coal mass/stoichiometric air mass}} \quad (7)$$

The temperature of the adiabatic combustion reaction reaches its peak when the equivalence ratio is 1.00. Our simulation is in agreement with the experimental result reported by Hankalin et al. (2011) (Hankalin et al. 2011). The deviation between the maximum temperature in this study (1691 °C) and the maximum temperature in Hankalin's study (1425 °C) is 15.73%, caused by the coal's proximate analysis and ultimate analysis differences.

However, the pattern between our simulation results and Hankalin's results is similar. Therefore, it is concluded that these simulations are valid. The highest temperature at equivalence ratio (ER) 1.0 is due to the complete oxidation reaction of fixed carbon, CO, and volatile matter in the stoichiometric conditions releasing optimum combustion energy. The lowest temperature of 1490 °C is at ER 1.08. By increasing ER from 0.63 to 1, the reaction approaches the perfect oxidation of fixed carbon, CO, and volatile matter in stoichiometric conditions. When the ER is lower than 1, the energy released during combustion will be diluted or distributed to the excess air causing decreasing in temperature. When the ER is higher than 1, the combustion process does

not complete and decreases the temperature.

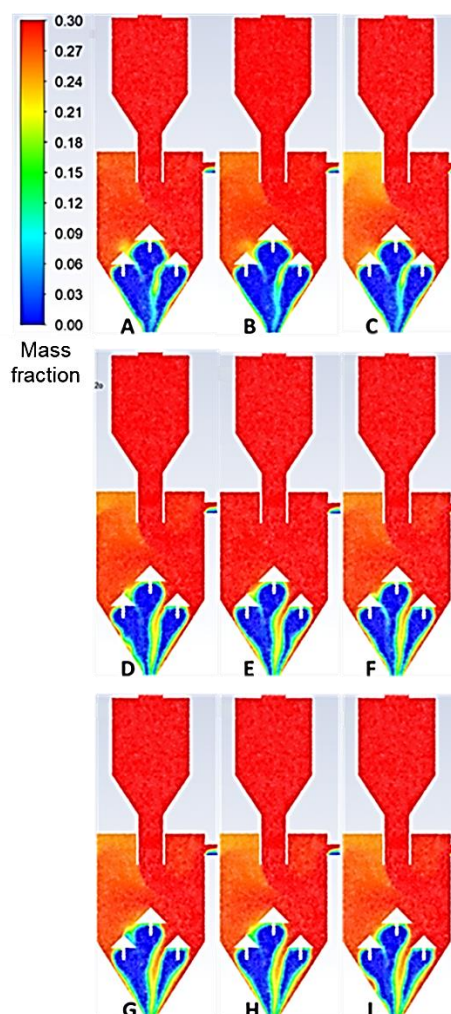


**Fig. 6:** Distribution of moisture content in Variable A (ER 0.63), B (ER 0.68), C (ER 0.74), D (ER 0.91), E (ER 1), F (ER 1.08), G (ER 1.1), H (ER 1.2), I (ER 1.31) in the steady-state

Figure 5 shows the steady-state temperature distribution. Temperature distribution varies from 26.85 to 1600 °C. The coal decomposition begins with releasing moisture on the coal surface and pore at 110-211 °C. Then, at the temperature of 211 °C to 420.8 °C, coal decomposes and devolatilize to produce volatile matter. Volatile matter begins to oxidize at the temperature of 420.8 °C (Borah et al. 2011). The combustion energy of volatile matter heated the input air leading to the coal moisture evaporation.

From all variables, variable B (Fig. 5b) generates the narrowest burning zone at temperature. The low burning zone protects the coal from being excessively combusted, but the heat is high enough to evaporate the moisture, as shown on the inlet cone temperature of 180 °C. ER close to stoichiometric conditions (Fig. 5c,d) produces a broader combustion zone compared to variables A and B (Fig. 5a-b). A high air velocity (43.75 m/s) will produce a better combustion process; however, this high rate locally reacts with the coal and generates a high temperature. Lowering air velocity to 29.96 m/s, which is close to ER of 1, the combustion area becomes wider because of the longer contact time. Decreasing the air velocity to 24.87 m/s does not significantly change the temperature profile even though the ER is higher than 1.

### **The effect of the equivalence ratio on moisture content distribution in a steady state system**

The heat of combustion is used to evaporate coal moisture. Therefore, the ER affects the coal moisture content distribution and determines the reduction percentage. The reduction of moisture content by releasing H<sub>2</sub>O molecules on the coal surface and pores happens at 110 °C to 211 °C.

Figure 6 shows the moisture content distribution profile. Blue contours under the cone do not imply the 0 value of moisture content but no coal under this zone because the cone spreads the coal through the edge of the coal dryer wall. From the profile, variable B shows lower moisture content compare to others. However, the coal outlet shows similar moisture content for variables A-B. Opposite to A-B, variable C-I shows relatively high moisture content. The moisture content profile only shows the

actual moisture content. However, because the coal flow rate is different, the calculation of the moisture content reduction efficiency is shown as

$$\text{moisture content reduction efficiency} = \frac{\text{coal feed moisture content (0.3)} - \text{output moisture content}}{\text{coal feed moisture content}} \times 100\% \quad (8)$$

Table 4 shows the relationship between the ER and the moisture content reduction efficiency. The reduction efficiency increases for ER of 0.63 to 0.74 but decreases for ER of 0.91 to 1.31. The optimum reduction efficiency was achieved at ER of 0.74 (variable C). The excess condition (ER of 0.63-0.91) produces higher efficiency than the lean condition (1.08-1.31) because a better combustion phenomenon occurs during the excess condition. However, even though this condition generates the highest moisture reduction efficiency, if the temperature distribution in Figure 4c was analyzed, high temperatures of 477.40 to 777.76 °C are detected in the upper part of the cone. This high temperature indicated that the coal was burned. Therefore, the optimal condition is variable B with ER of 0.64 because the reduction efficiency is relatively high, but the temperature distribution is good enough. Figure S2 shows the moisture content of variables A to variable I in the line position of the coal dryer. From this graph, the moisture content starts to decrease at the height of 7 m. The outlet of the coal dryer is at 10.5 meters.

### **The effect of the equivalence ratio on the distribution of volatile matter, oxygen and carbon dioxide in a steady-state system**

High volatile content in fuel is undesirable because it produces more tar, causes

problems in internal combustion engines, especially explosion hazards, and reduces the percentage of fixed carbon (Miller 2013). We observe the distribution of Volatile Matter (VM) in coal to determine the VM percentage reduction. Volatile matter is usually a mixture of aromatic hydrocarbons, short and long-chain hydrocarbons, and sulfur gas. Volatile matter consists of flammable gases such as hydrogen (H), carbon monoxide (CO), and methane (CH<sub>4</sub>) (Kumar and Anand 2019). Figure 7 shows the distribution of VM. The reduction of volatile matter is due to an oxidation reaction with oxygen at 420.8 °C. At the outlet, the VM is almost close to 0 for the ER value of less than 1 (excess condition). The excess air leads to the complete combustion of Volatile Matter, so there is a significant reduction in Volatile Matter. The high content of VM in Figure 7c and high temperature in Figure 5c are in agreement, indicating that coal combustion happens. Low ER (A-C) shows no volatile matter in the outlet because excess air reacts completely with VM. For ER relatively close to 1.0, the volatile matter tends to increase and remain in the coal dryer outlet. This tendency is similar to oxygen and carbon dioxide (Figures S3 and S4). The volatile matter will react with oxygen to produce carbon dioxide. Therefore rich oxygen is only in the under cone zone (Figure S4). The carbon dioxide shown in Figure S4c validates that the combustion happens in the upper side of the coal dryer.

### **The effect of the equivalence ratio on the distribution of fluid velocities in a steady-state system**

The vector velocity of fluid particles and coal dryer determine the velocity and direction of fluid flow. This flow influences the combustion reaction. Figure 8 shows almost

no difference between each variable so that the equivalence ratio does not affect the distribution of fluid velocity. The fluid flows from above the coal inlet area downward due to gravity's influence, and a vortex flow is formed in the upper bin of the coal dryer. A dead zone of coal particles is formed on the left and right sides of the coal dryer top bin (black circle). Coal in the dead zone is difficult to exit the dryer. The gas outlet velocity is in the range of 43-48 m/s. This high velocity is due to the volume shrinking in the outlet. Herein, it is concluded that variable B is the best process variable. Furthermore, the unsteady state simulation was analyzed to observe the drying and combustion process more deeply.

### **Unsteady state modeling approach in the Coal Dryer**

Variable B was chosen to do the unsteady state simulation because of the optimal conditions obtained in variable B. This simulation uses 4000 iterations and produces 220 seconds. Figure 9 shows the unsteady state temperature distribution of variable B. The temperature distribution shows a lower limit of 26,716 °C to an upper limit of 1570 °C.

The input coal has a temperature of 26.7 °C. After 5 to 150 seconds of combustion, it produces temperatures of up to 1570 °C in a small part of the coal dryer area. In Figure 15, there is a process of decomposition of the coal material starting with the release of water content on the surface of the coal, and at the coal pores, it takes place between 110 °C to 211 °C. In the temperature area of 211 °C to 420.8 °C, it is decomposition or devolatilization of coal Volatile Matter levels (Borah et al. 2011).

**Table 4.** Effect of Equivalence Ratio on the efficiency of moisture

| <b>Variable</b> | <b>Line</b> | <b>Final moisture content (mass fraction)</b> | <b>Average final moisture content (mass fraction)</b> | <b>% Efficiency of moisture content reduction</b> | <b>Equivalence ratio</b> |
|-----------------|-------------|---|---|---|--------------------------|
| A               | line A      | 0.0528  | 0.0438  | 85.41   | 0.63                     |
|                 | line B      | 0.0413  |   |   |                          |
|                 | line C      | 0.0413  |   |   |                          |
|                 | line D      | 0.0398  |   |   |                          |
| B               | line A      | 0.0342  | 0.0409  | 86.37   | 0.68                     |
|                 | line B      | 0.0496  |   |   |                          |
|                 | line C      | 0.0322  |   |   |                          |
|                 | line D      | 0.0476  |   |   |                          |
| C               | line A      | 0.0308  | 0.0382  | 87.28   | 0.74                     |
|                 | line B      | 0.0476  |   |   |                          |
|                 | line C      | 0.0291  |   |   |                          |
|                 | line D      | 0.0450  |   |   |                          |
| D               | line A      | 0.0446  | 0.0623  | 79.24   | 0.91                     |
|                 | line B      | 0.0838  |   |   |                          |
|                 | line C      | 0.0421  |   |   |                          |
|                 | line D      | 0.0786  |   |   |                          |
| E               | line A      | 0.0463  | 0.0683  | 77.24   | 1.00                     |
|                 | line B      | 0.0935  |   |   |                          |
|                 | line C      | 0.0435  |   |   |                          |
|                 | line D      | 0.0897  |   |   |                          |
| F               | line A      | 0.0430  | 0.0671  | 77.65   | 1.08                     |
|                 | line B      | 0.0946  |   |   |                          |
|                 | line C      | 0.0410  |   |   |                          |
|                 | line D      | 0.0896  |   |   |                          |
| G               | line A      | 0.0451  | 0.0928  | 69.08   | 1.10                     |
|                 | line B      | 0.1445  |   |   |                          |
|                 | line C      | 0.0436  |   |   |                          |
|                 | line D      | 0.1378  |   |   |                          |
| H               | line A      | 0.0689  | 0.1063  | 64.55   | 1.20                     |
|                 | line B      | 0.1481  |   |   |                          |
|                 | line C      | 0.0663  |   |   |                          |
|                 | line D      | 0.1421  |   |   |                          |
| I               | line A      | 0.0705  | 0.1089  | 63.70   | 1.31                     |
|                 | line B      | 0.1517  |   |   |                          |
|                 | line C      | 0.0682  |   |   |                          |
|                 | line D      | 0.1451  |   |   |                          |

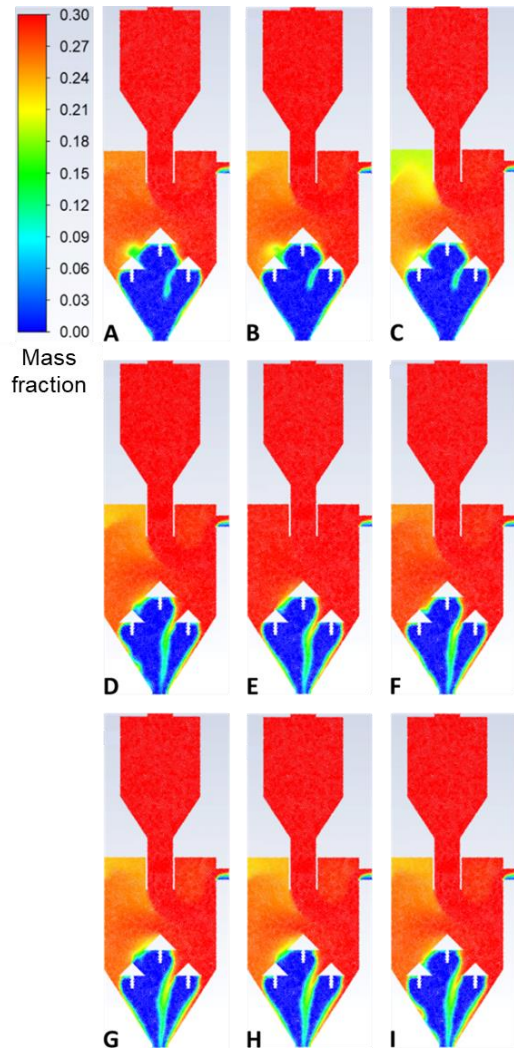
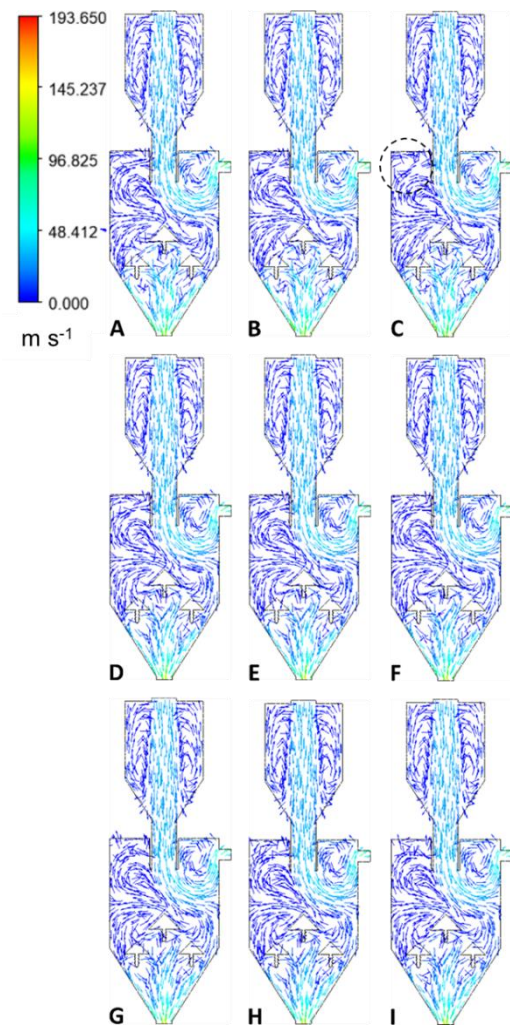


**Fig. 7:** Distribution of volatile matter for variable A (ER 0.63), B (ER 0.68), C (ER 0.74), D (ER 0.91), E (ER 1), F (ER 1.08), G (ER 1.1), H (ER 1.2), I (ER 1.31) in the steady-state

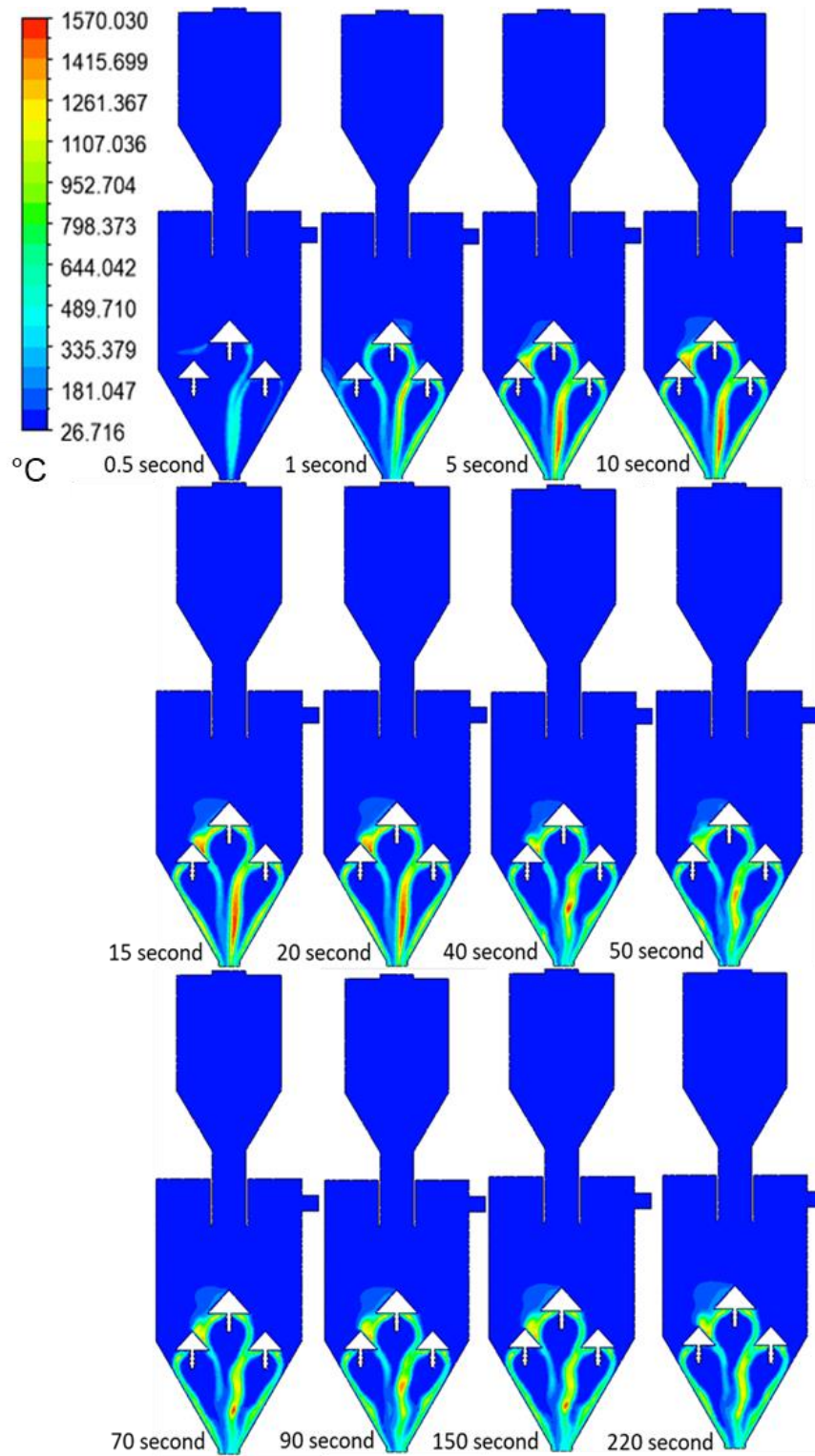
Furthermore, at a temperature of 420.8 °C, the oxidation process of Volatile Matter begins. The combustion of Volatile Matter occurs with oxygen, followed by the burning of fixed carbon with oxygen. After 0.5 seconds, moisture content evaporates from part of the coal, and the volatile matter has been partially burned, increasing the temperature to 489.71 °C.

Figure 9 show the combustion of volatile matter (indicated by high temperature) and reduced moisture content in the same zone.

After 10 seconds, the red area expanded to the left side of the middle cone. The temperature is almost constant after 40 s and fluctuates around 952.7 °C, creating an oscillation. This oscillation is caused by the movement of coal particles, in agreement with the report of Salinero et al. (2018) (Salinero et al. 2018).



**Fig. 8:** Distribution of the direction of movement of the particles of variable A (ER 0.63), B (ER 0.68), C (ER 0.74), D (ER 0.91), E (ER 1), F (ER 1.08), G (ER 1.1), H (ER 1.2), I (ER 1.31) in a steady-state



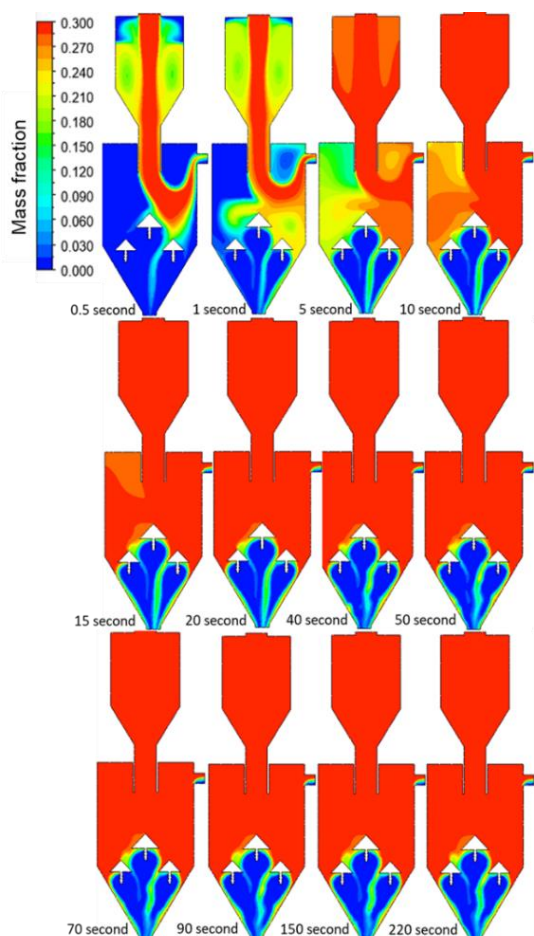
**Fig. 9:** Temperature Distribution of variable B in the unsteady state condition

Figure 10 shows a temperature oscillation of the pilot plant coal dryer. The data shows

an agreement between simulation and experiment.

### Unsteady state distribution of Moisture Content

The unsteady distribution was observed to determine the moisture content reduction in coal as a function of time. The reduction of moisture content in coal occurs due to the release of H<sub>2</sub>O molecules (evaporation) on the surface of the coal and in the coal pores. This phenomenon takes place between 110 °C to 211 °C. As shown in Figure 11, after 0.5-1 s, water evaporates, and the volatile matter and coal have been partially burned, increasing the temperature to 489.71 °C. There is a vortex flow in the bottom bin which causes a reduction in moisture content. This vortex facilitates low humid air, and high humid coal in contact leads to mass transfer of H<sub>2</sub>O from coal to the air.



**Fig. 10:** Distribution of moisture content in Variable B under unsteady state conditions

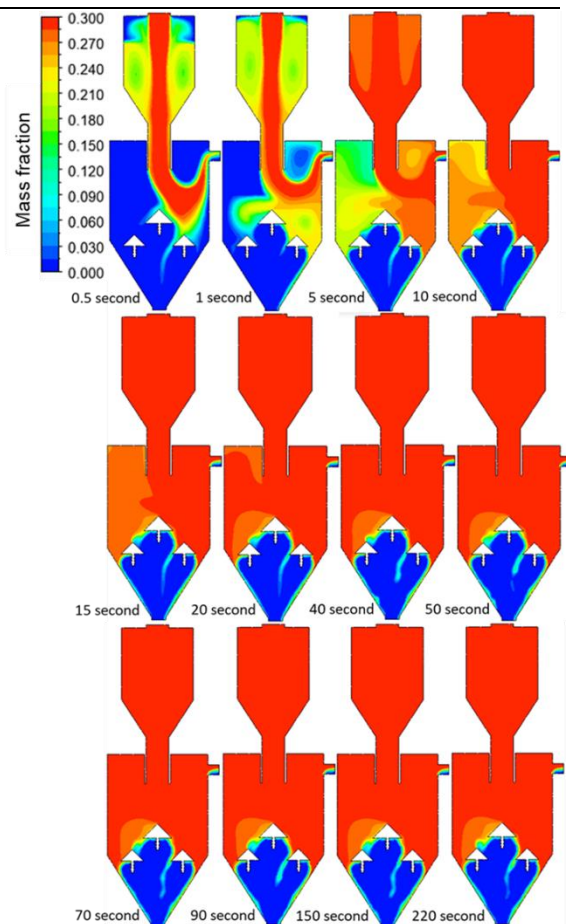


**Fig. 11:** Distribution of Volatile Matter for Variable B under unsteady state

At this 0.5s, the H<sub>2</sub>O fraction in the lower bin is not evenly distributed, and the coal has not fully occupied the space in the bottom bin. Then from 1-15 s, the moisture content fraction at the top of the bin increased from 0.21 to 0.3. The coal has occupied all parts of the coal dryer after 15 s and has experienced an oxidation reaction of burning coal around the cone. After 15 s, the red area expanded on the cone top (transform from yellow to red) so that there was an increase in the H<sub>2</sub>O fraction with a range of 0.27 to 0.3. After 20 s, the process achieved a steady condition. At the bottom of the air inlet cone, there was a reduction in moisture content with an average value of 0.04, as shown in Table 4, with a reduction in moisture content percentage of 86.3%.

---

### **Unsteady state distribution of Volatile matter, oxygen and carbon dioxide**

Figure 12 shows the contours of the Volatile Matter fraction. The Volatile Matter fraction on the bin increases at 1-5 s. This is because the coal has filled the bin at the top of the coal dryer. Initially, volatile matter flows to the gas outlet due to lower pressure. After the reaction starts at 15-220 s, the red area increases and is evenly distributed in the top bin. After 220 seconds no change in the Volatile Matter fraction, indicating the process is already in a steady state.

Figure S5 shows the distribution of oxygen gas flow that occurs in the coal dryer. At 0.5 seconds, the air fraction decreases due to the combustion reaction of Volatile Matter and part of the coal. The right side shows a blue zone indicating oxygen has reacted with the volatile matter in agreement with the CO<sub>2</sub> analysis of Figure S6. In the 1-10 s, the air fraction increases due to the continuous flow rate of air. After 0.5 s, the oxygen distribution is in steady conditions.

In the upper bin, no mass fraction of O<sub>2</sub> shows that the oxidation reaction occurs at the bottom of the air inlet cone. Compared with the distribution of CO<sub>2</sub> in Figure S6, the CO<sub>2</sub> distribution zone covers the outer part of the O<sub>2</sub> distribution. CO<sub>2</sub> compound has been formed marked with a light blue contour at the bottom of the air inlet cone at 0.5 s. The Blue zone on the right side of the cone indicates that oxygen has reacted with the volatile matter supported by the formation of CO<sub>2</sub> gas in the zone. Then at 1 s, the mass fraction of CO<sub>2</sub> increases at the bottom of the cone area, and at 1-5 seconds, the area of the CO<sub>2</sub> zone expands. The area above the cone does not show CO<sub>2</sub> gas formation. After 5 seconds, the system reaches a steady-state state.

### **CONCLUSIONS**

The CFD simulation results can represent the phenomenon of coal drying in a coal dryer which can be theoretically validated. In excess air, it shows a better quality of combustion and higher moisture content reduction. The lower air velocity will cause low combustion performance, and reduction of moisture content is not optimal. We found that the best flow rate of coal, air velocity, and equivalence ratio to obtain high moisture reduction performance is 6.51 kg/s, 43.75 m/s, and 0.63, respectively. The temperature and pattern generated from the simulation and pilot plant results are in agreement. The coal drying process is promising to reduce moisture content with a high reduction and low moisture outlet of 0.0409 (mass fraction).

### **ACKNOWLEDGEMENT**

We thank Universitas Internasional Semen Indonesia for its support in this research.

### **CONFLICT OF INTEREST**

The authors declare no conflict of interest.

### **AUTHORS' CONTRIBUTIONS**

AH: supervise, revise and write initial manuscript.

AAW and CDW: conduct CFD simulation.

FM: Supervise.

ELS: Supervise the CFD simulation and pilot plant experiment.

### **AVAILABILITY OF DATA AND MATERIALS**

Data and materials are available upon request.

---

**APPENDIX**

|                      |  |
|----------------------|--|
| $\rho$               | : Density  |
| $\varepsilon$        | : Dissipation rate   |
| $\sigma_\varepsilon$ | : The turbulent Prandtl number for $\varepsilon$   |
| $\sigma_k$           | : The turbulent Prandtl number for $k$   |
| $\mu$                | : Viscosity  |
| $\mu_t$              | : Turbulent viscosity  |
| $\bar{\tau}$         | : Stress tensor  |
| $\bar{\tau}_{eff}$   | : Effective stress tensor  |
| $C_{1\varepsilon}$   | : Constant   |
| $C_{2\varepsilon}$   | : Constant   |
| $C_{3\varepsilon}$   | : Constant   |
| $E$                  | : Energy (Internal energy, potential energy, and kinetic energy)   |
| $F$                  | : External body force  |
| $g$                  | : Gravity  |
| $G_b$                | : Generation of turbulence kinetic energy due to buoyancy  |
| $G_k$                | : Generation of turbulence kinetic energy due to the mean velocity gradients                             |
| $h_j$                | : Sensible heat for species j  |
| $J_i$ and $J_j$      | : Diffusion flux of species I and j respectively   |
| $k$                  | : Turbulence kinetic energy  |
| $k_{eff}$            | : Effective conductivity   |
| $p$                  | : Pressure   |
| $R_i$                | : Net production rate of species I by chemical reaction  |
| $S_\varepsilon$      | : User-defined source for $\varepsilon$  |
| $S_h$                | : The heat generation rate from chemical reactions or user-defined related to the volumetric heat source |
| $S_i$                | : The rate of creation by addition from the dispersed phase and any user-defined sources                 |
| $S_k$                | : User-defined source for $k$  |
| $S_m$                | : Mass added to the continuous phase from the dispersed second   |

phase

|                 |   |
|-----------------|---|
| $T$             | : Temperature   |
| $t$             | : Time  |
| $u_i$           | : The velocity of species i   |
| $v$             | : Velocity  |
| $x_i$ and $x_j$ | : x and y coordinate for species i and j  |
| $Y_i$           | : Mass fraction of species i  |
| $Y_M$           | : The contribution of the fluctuating dilatation in the compressible turbulence to the overall dissipation rate |

**REFERENCES**

- ANSYS Inc. (2020) ANSYS Fluent Theory Guide. ANSYS, Inc, Canonsburg
- Arena U (2013) 17 - Fluidized bed gasification. In: Scala FBT-FBT for N-ZEC and G (ed) Woodhead Publishing Series in Energy. Woodhead Publishing, pp 765–812
- Auamwong S, Srinophakun TR. (2020). "Mathematical Model for Agglomeration Process of Milk Powder." *ASEAN J. Chem. Eng.*, 20,154–164.
- Baaqy L Al, Arias G, Rachimoellah M, Nenu RKT. (2013). "Pengeringan Low Rank Coal dengan Menggunakan Metode Pemanasan tanpa Kehadiran Oksigen." *J. Tek. Pomits*, 2,228–233
- Borah RC, Ghosh P, Rao PG. (2011). "A review on devolatilization of coal in fluidized bed." *Int. J. Energy Res.*, 35,929–963.
- Canbek O, Erdoğan ST. (2020). "Influence of production parameters on calcium sulfoaluminate cements." *Constr. Build Mater.*, 239,117866.
- ESDM. (2018). "Cadangan Batubara Indonesia Sebesar 26 Miliar Ton." In: Kementerian. Energi dan Sumber Daya Miner. <https://www.esdm.go.id/id/media-center/arsip-berita/cadangan-batubara->

- 
- indonesia-sebesar-26-miliar-ton.  
Accessed 17 May 2021
- Grimes RW, Cha CY, Sheesley DC. (1990). "Preparation for upgrading western subbituminous coal." Laramie, Wyoming
- Halim A, Kusumandari FA, Widiyastuti, et al. (2013). "The rule of carrier gas flow rate to Li<sup>+</sup> diffusivity of LiFePO<sub>4</sub> particles as lithium battery application." In: 2013 International Conference on Renewable Energy and Sustainable Energy (ICRESE). pp 170–174
- Halim A, Setyawan H, Machmudah S, et al. (2014). "Effect of fuel rate and annealing process of LiFePO<sub>4</sub> cathode material for Li-ion batteries synthesized by flame spray pyrolysis method." *AIP Conf. Proc.* 1586,173–178.
- Hankalin V, Helanti V, Isaksson J (2011) "High efficiency power production by gasification". In: Cossu R, He P, Kjeldsen P, et al. (eds) Sardinia 2011-Thirteenth International Waste Management and Landfill Symposium. CISA Publisher, Cagliari
- Jovanovic R, Milewska A, Swiatkowski B, et al. (2011). "Numerical investigation of influence of homogeneous/heterogeneous ignition/combustion mechanisms on ignition point position during pulverized coal combustion in oxygen enriched and recycled flue gases atmosphere." *Int. J. Heat Mass Transf.*, 54,921–931.
- Kumar M D R, Anand R. (2019). "Chapter 5 - Production of biofuel from biomass downdraft gasification and its applications". In: Azad AK, Rasul MBT-AB (eds) Woodhead Publishing Series in Energy. Woodhead Publishing, pp 129–151
- Li H, Zhang S, Li Y, et al. (2017). "Numerical Simulation and Experimental Research on Drying Behavior of a Single Lignite Particle (SLP) under High-Temperature Flue Gas." *Energy and Fuels*, 31,13329–13337.
- Li X, Gao L, Yun D, et al. (2018). "A CFD modeling investigation for structure optimization of a rotary steam tube dryer." *IOP Conf. Ser. Mater. Sci. Eng.*, 397,12076.
- Li ZK, Yan HL, Yan JC, et al. (2019). "Drying and depolymerization technologies of Zhaotong lignite: A review." *Fuel Process Technol.*, 186, 88–98.
- Liu M, Xu C, Han X, et al. (2020). "Integration of evaporative dryers into lignite-fired power plants: A review." *Dry Technol.* 38, 1996–2014.
- Marshall EM, Bakker A. (2003). "Computational Fluid Mixing." *Handb. Ind. Mix.* 257–343
- Miller B. (2013). "3 - Fuel considerations and burner design for ultra-supercritical power plants." In: Zhang DBT-U-SCPP (ed) Woodhead Publishing Series in Energy. Woodhead Publishing, pp 57–80
- Ohm T-I, Chae J-S, Lim J-H, Moon S-H. (2012). "Evaluation of a hot oil immersion drying method for the upgrading of crushed low-rank coal." *J. Mech. Sci. Technol.*, 26,1299–1303.
- Osman H, Jangam S V, Lease JD, Mujumdar AS. (2011). "Drying of Low-Rank Coal (LRC)—A Review of Recent Patents and Innovations." *Dry Technol.*, 29, 1763–1783.
- Phiciato P, Yaskuri D. (2019). "Dual-Stage Drying Process of Lignite Using Pilot Scale Coal Rotary Dryer." *Int. J. Coal Prep. Util.* 39, 373–388.
- Rao Z, Zhao Y, Huang C, et al. (2015). "Recent developments in drying and dewatering for low rank coals." *Prog. Energy Combust. Sci.*, 46,1–11.
-

- Salinero J, Gómez-Barea A, Fuentes-Cano D, Leckner B. (2018). "Measurement and theoretical prediction of char temperature oscillation during fluidized bed combustion." *Combust. Flame*, 192, 190–204.
- Si C, Wu J, Zhang Y, et al. (2019). "Experimental and numerical simulation of drying of lignite in a microwave-assisted fluidized bed." *Fuel*, 242, 149–159.
- Simanjuntak ME, Prabowo, Widodo WA, et al. (2019). "Experimental and numerical study of coal swirl fluidized bed drying on 100 angle of guide vane." *J. Mech. Sci. Technol.*, 33, 5499–5505.
- Siripaiboon C, Sarabhorn P, Areeprasert C. (2020). "Two-dimensional CFD simulation and pilot-scale experimental verification of a downdraft gasifier: effect of reactor aspect ratios on temperature and syngas composition during gasification." *Int. J. Coal Sci. Technol.*, 7, 536–550.
- Xu Y, Musser J, Li T, et al. (2018). "Numerical Simulation and Experimental Study of the Gas-Solid Flow Behavior Inside a Full-Loop Circulating Fluidized Bed: Evaluation of Different Drag Models." *Ind. Eng. Chem. Res.*, 57, 740–750.
- Yadav S, Mondal SS. (2019). "A complete review based on various aspects of pulverized coal combustion." *Int. J. Energy Res.*, 43, 3134–3165.
- Yang X, Chen G, Huang L, et al. (2021). "Experimental study on bituminous coal blending in a down-fired boiler with anthracite combustion system under low load." *Asia-Pacific J. Chem. Eng.*, e2676.
- Zhang K, You C. (2013). "Numerical simulation of lignite drying in a packed moving bed dryer." *Fuel Process Technol.* 110, 122–132.
-